

Axisymmetric whole pin life modelling of advanced gas-cooled reactor nuclear fuel

R. Mella^(a) and M. R. Wenman^(a*)

(a) Department of Materials, Imperial College London, London, SW7 2AZ

(a*) Corresponding author: Tel +44 (0)207 5946763 E-mail: m.wenman@imperial.ac.uk

Abstract

Thermo-mechanical contributions to pellet-clad interaction (PCI) in advanced gas-cooled reactors (AGR) are modelled in the ABAQUS finite element (FE) code. User supplied sub-routines permit the modelling of the non-linear behaviour of AGR fuel through life. Through utilization of ABAQUS's well-developed pre- and post-processing ability, the behaviour of the axially constrained steel clad fuel was modelled. The 2D axisymmetric model includes thermo-mechanical behaviour of the fuel with time and condition dependent material properties. Pellet cladding gap dynamics and thermal behaviour are also modelled. The model treats heat up as a fully coupled temperature-displacement study. Dwell time and direct power cycling was applied to model the impact of online refuelling, a key feature of the AGR. The model includes the visco-plastic behaviour of the fuel under the stress and irradiation conditions within an AGR core and a non-linear heat transfer model. A multiscale fission gas release model is applied to compute pin pressure; this model is coupled to the PCI gap model through an explicit fission gas inventory code. Whole pin, whole life, models are able to show the impact of the fuel on all segments of cladding including weld end caps and cladding pellet locking mechanisms (unique to AGR fuel). The development of this model in a commercial FE package shows that the development of a potentially verified and future-proof fuel performance code can be created and used.

Keywords: Fuel Performance, ABAQUS, Finite Element, AGR

1.0 Introduction

1.1 Pellet-cladding interaction

Numerous authors have investigated the phenomenon of PCI in the past [1–10]. These studies have included the AGR system. The AGR studies from the early 90s offer insight into the effective bonding forces between AGR cladding and fuel, albeit that these studies were for a very simplified geometry and material properties. Walker's models were two dimension r - θ segments of a pellet and cladding in a coupled thermo-mechanical transient analysis. This analysis showed that the expected bond between pellet and clad will fail and cause the debonding of about 6% of the pellet-clad surface producing sufficient stress relief to prevent further debonding. Walker also shows that a failure of this size was sufficient to cause a two orders of magnitude reduction in the number of pellet cracks to propagate in the adjacent cladding. Most work in recent years has focussed on water cooled systems [2-3, 11-13]. Marchal [11] showed through 3D modelling of PCI, in the CAST3M FE code, that the while pellet fracture did produce stress concentrations in the cladding there was also a significant stress remaining in the fuel fragment. These pellet fragments had sufficient remaining stresses that later interaction with the cladding through friction contact produced further radial cracking. Marchal's smeared crack model emphasises the non-linear behaviour of PCI cracking and that it is strongly dependent on fuel-cladding friction.

Very recently attempts have been made to use more openly available commercial FE codes to model fuel performance [12], this was to serve as a test bed for a custom fuel performance model [13]. Williamson modelled the PWR system using an axisymmetric model and showed the cladding stresses for PWR fuel can be computed. With modification the model was capable of including thermal-mechanical behaviours of the highly non-linear material responses, which contribute to the fuel pin response. Williamson's model included effects of fission gas release and its impact on pin pressure. Capable of both steady state and transient studies displaying an ability to match the capabilities of current fuel performance codes in commercial modelling packages.

A whole variety of bespoke fuel performance codes are also available spanning different numbers of dimensions [14] and also often specialising in steady state event modelling (e.g. FRAPCON [15] and COMETHE) problems or transients (e.g. FRAPTRAN[16] and TRANSURANUS [17]) whilst others give overall pin performance for long timescales. ENIGMA, for example, is intended for the analysis of normal operation and frequent faults [18]. Many of the fuel performance codes also rely heavily on empirical data and as such are not necessarily able to predict well events outside of the envelope for which they were created. A good example that illustrates this was the FUMEX-II research project on fuel behaviour predictions at high burn-up [19]. The experiment showed the varied results obtained by many fuel performance codes trying to predict the same problem when designed for different fuel types and problems, arising from data gaps especially at high burn-up, and different fitting approaches on empirical data. One way to get around this is to try, where possible, to make fuel performance codes based on physical laws rather than empirically derived data making them as mechanistic as possible. Similarly to Williamson this was the aim of this work albeit for the case of modelling PCI in AGR fuels. Furthermore, the objective was to try to use ABAQUS, which now has enough features to allow a good representation of many of the needed phenomena, such as heat transfer, diffusion, gap elements etc to deal with the complicated problems of fuel performance. Presented within this paper is a coupled fuel-gap-clad heat transport axisymmetric whole pin model for the AGR.

1.2 The AGR system

The AGR core contains about 300 fuel stringers. Each stringer contains seven or eight 1 m long sub-assemblies containing 36 steel clad fuel pins. Fuel pins consist of stainless steel tubes made from Nb stabilised austenitic stainless steel (25 wt% Ni, 20 wt% Cr, 0.05 wt% C and 0.5 wt% Nb) containing about 64 annular UO₂ ceramic pellets enriched in ²³⁵U by several per cent. Due to the relatively high temperatures of 650°C – 700°C and overpressure (4MPa) of the CO₂ coolant in the core, the cladding creeps down until initial contact with the pellet occurs. This happens very early in life (over a timescale of days to weeks) compared to the behaviour of PWR fuel and is in part a consequence of the fast cladding creep rate, at the high operating temperature, and a smaller initial pellet cladding gap (20 µm) than that of a PWR. In the case of a power increase this PCI can induce large stresses in the cladding that might lead to fuel pin failure. It is therefore necessary to be able to understand the occurrence of PCI failure. The AGR fuel also does not have the capacity to freely expand during power ramping as there is no plenum at the top of the fuel pins. As the fuel temperature ramps up the thermal expansion of the pellets stretches the steel cladding to accommodate the increase in length. In order to ensure a near uniform strain along the axial length of the fuel pin the cladding is deformed into grooves, known as anti-stacking grooves (ASG), manufactured into some of the pellets. The cladding is

formed into these ASGs at manufacture to lock together approximately five pellet groups and this helps prevent large gaps forming in the fuel stack due to the pellets restacking (see, Fig. 1).

Since the year 2000 there have been several fuel failures potentially attributable to PCI in various AGR reactors [20]. When radioactivity in the coolant gas indicates that fuel in the reactor may have failed, the operators have to follow a procedure that may involve reducing reactor power or shutting it down. The potential costs include: replacement for generation loss, non-optimum use of fuel and increased fuel disposal costs as failed fuel cannot be disposed of by the normal route. These include: reduction in reactor power, not refuelling on-load (a feature of the AGR system) and not shuffling fuel (to improve utilisation). FE simulations shown here are used to help in interpreting experiments and ultimately to develop efficient fuel codes, core protections and PCI resistant designs.

2.0 Model development

The choice of an axisymmetric model permits the modelling of an entire AGR fuel pin through life. The pin was assumed to be axially symmetric about its centre to reduce computation time. The model pin contains 32.5 pellets of various geometries and materials. The grooved locking pellets are introduced every five conventional pellets, and the cladding is collapsed into the ASGs producing regions where the pellets are mechanically locked together. Before the pin end caps there is a third type of pellet, an alumina (Al_2O_3) spacer pellet. The alumina pellets act primarily as a thermal insulator for the fuel pin end caps and welds.

To carry out these studies the commercial FE package ABAQUS [21] was used. The major focus of this study was the use of the ABAQUS/Standard implicit code solving initially a transient coupled heat and displacement problem to accurately model heat up behaviour of the fuel pin. The model was then solved in the steady state for long term effects such as creep and any direct power cycling to simulate the online refuelling was solved in transients in order to study the impact on the AGRs cladding stresses. Implicit numerical methods and sophisticated iteration and time integration error control permit simulation of steady reactor operation, or very rapid transients.

Each pellet was constructed from quadrilateral linear axisymmetric coupled temperature and displacement elements, the cladding is modelled with linear triangular elements allowing for adaptive remeshing in ABAQUS (quadrilateral elements are unsupported in automatic adaptive remeshing). The mesh of the pellets and cladding are shown in Fig. 2. The size of element within each pellet ranges from 150 μm to 200 μm . The steel cladding was meshed consistently with elements of the same type but element sizes ranged from 50 μm to 20 μm . Mesh sensitivity in the cladding was addressed by the use of adaptive remeshing with a minimum element size of 1 μm and 3 ABAQUS error indicators: Mises equivalent stress, equivalent plastic strain and the creep strain. Meshes containing elements below 50 μm produced only small errors in the stress of the order of several hundred Pa. Final remeshing was manual from observation of error indicators. Manual remeshing was used as surface elements, which are required for modelling the fuel pin as a fluid filled cavity, are not supported in an automatic remeshing procedure (ABAQUS 6.10).

The reduced dimensions of the axisymmetric model permit a higher element density when compared to a 3D fuel model; for the cladding a characteristic element size of less than 50 μm

was used. Even at this high mesh density a model spanning large timescales was possible. A whole five year fuel dwell time was modelled on a single core workstation in a matter of an hour. The model was scaled to years of fuel pin life. Despite the complex contact that may occur during ramping an implicit FE method was used (ABAQUS/Standard) with adaptive time stepping. A minimum time step of 10 μ s and a maximum of 10 days were used; the upper limit on time stepping was large because of the ability to sub-cycle the fission product inventory and fission gas release models. After a one week heat-up to full volumetric power of 125 MW/m³ the fuel was held at this power for one year, followed by the application of power cycles (3 cycles between 30% to 70%) to the fuel pin to model online refuelling, this operation was preceded by a power spike to 150% volumetric power. Finally, the fuel was modelled in a steady state manner at 100% power for the remainder of a 5 year dwell time (see, Fig. 3 for load history). The overall model parameters are given in Table 1.

2.1 Gap and contact models

The clad-pellet gaps variable nature requires a model that couples the mechanics of the fuel pellet and cladding with a model for the gas gap. Material models are applicable at early life and extensible to late life operation. ABAQUS includes robust contact algorithms applicable to arbitrary geometry, essential for capturing all the complexity of multidimensional pellet-pellet or PCI contact.

Heat transport between the different surfaces within the fuel pin was implemented by use of gap elements with properties defined by the URGAP model [22,23] assuming that at early life the cladding inner and fuel outer surfaces are quite smooth (0.8-2 μ m surface roughness). For late life a coupled fission gas release and fission gas inventory model is used to compute gas content and this is also implemented in ABAQUS. This internal model supplies the appropriate fractions of filling gas (helium, krypton and xenon) in order to compute gap conductivity. The external pin surfaces are modelled by a gas film representing turbulent flow of the CO₂ coolant, with a sink temperature, which increases linearly over heat up time from 650°C to the expected outlet temperature of the AGR of approximately 700°C.

$$h_{gap} = h_{rad} + h_{cond} + h_{press} \quad 2.1$$

$$h_{cond} = \frac{k_g}{d_g + 1.5 * (R_f + R_c) + g_f + g_c} \quad 2.2$$

$$h_{press} = C_s \frac{2k_f k_c}{k_f + k_{cl}} \frac{P}{\delta^{1/2} H} \quad 2.3$$

$$k, \frac{\partial k}{\partial d}, \frac{\partial k}{\partial p}, \frac{\partial k}{\partial T_A}, \frac{\partial k}{\partial T_B} \quad 2.4$$

The URGAP model includes different heat transfer mechanisms as the sum of their heat transfer coefficients (radiative, h_{rad} , gas conduction, h_{cond} , of filling gas and pressure enhanced heat transfer, h_{press} expressed in equations 2.1 – 2.3). Where k_f, k_g and k_{cl} are the fuel, filling gas and cladding thermal conductivity respectively. Where g_f, g_c, R_f, R_c and d_g are the fuel and cladding accommodation length; fuel and cladding mean roughness and the gap thickness

respectively. C_s , P , T_A, T_B and H are the surface contact fraction (taken as $1 \text{ m}^{-1/2}$ as recommended from a fit to measurements [24]), contact pressure, temperature on fuel outer surface, temperature on inner cladding surface and cladding hardness respectively. The appropriate gas fraction mixing weighting factors were calculated according to Lindsay and Bromley [25].

The ABAQUS implementations of these interactions are in a GAPCON user sub-routine. This sub-routine takes as input the Jacobian matrix of the heat transfer contributions, which are to be included into the system matrix, which describes the thermal interactions between a slave surface node and a master surface node. By supplying ABAQUS with Jacobian matrix contributions (see equation 2.4), of changes of thermal conductivity with respect to surface clearance, contact pressure and the surface temperatures, a converged solution of thermal flux is more easily found. The radiative contributions were computed with ABAQUS's standard gap radiation toolset as accurate radiative calculations require view factor information not supplied in the GAPCON interface.

Mechanical contact, normal to a surface, is modelled as hard contact enforced through the penalty method, with separation permitted after contact, and the tangential mechanical contact behaviour is modelled as Coulombic friction where the steel/ UO_2 coefficient of friction, μ is 0.8. The thermal and mechanical interaction was used to define contact in pellet-pellet and pellet clad events. When modelling the fuel bonded to the cladding, the fuel and cladding are not permitted to separate (normal no separation contact constraint) and the tangential behaviour is a rough contact condition.

The filling gas pressure is modelled as a surface pressure arising from modelling the interior of the fuel pin as a "fluid" filled cavity, with hydrostatic boundary conditions, where the gas is a user defined volume. The free volume of the fuel pin is calculated from the evaluation of the internal pressure and this is found from the total pin volume minus the volume of each pellet. The process by which this is implemented in ABAQUS is through defining the surface encasing a pellet as a fluid filled vessel. This surface deforms with the surface nodes of the pellet changing volume with swelling and thermal expansion. Similarly the internal surface of the pin cladding is defined as the boundary of a fluid filled vessel, subtracting the pellet volumes from the total pin volume we have the pin free volume as a function of both pellet and cladding deformation. The pressure is defined by the inner pellet radius temperature and gas content as dictated by the fission gas release routines. Released fission gas is treated as an ideal gas.

The fuel pins exterior pressure is modelled as a simple surface pressure dictated by CO_2 coolant pressure approximated in the AGR core, which varies with external coolant temperature, permitting a complete model of fuel pin behaviour under normal and accident conditions while minimising assumptions on the boundaries of the computational domain.

2.2 RADAR model

In order to model long life behaviour of nuclear fuel considerations must be made towards power profiles. As nuclear fuel burns-up the ^{235}U content reduces and some of the fertile ^{238}U transmutes to various plutonium isotopes (particularly at the edge of the fuel pellet where the fastest flux exists). ABAQUS currently lacks the ability to compute neutron diffusion, to evaluate the flux for inventory change, and as there is power rating influence on species diffusion, in reality, ABAQUS cannot evaluate a many species diffusion-thermo-mechanical problem in a

coupled manner. To solve in ABAQUS would require custom elements or a small step iterative solution procedure.

The flux, power depression factors and uranium content was evaluated on a 2D uniform finite difference grid of similar dimensions to the fuel pin. RADAR [26] [27] is then explicitly time stepped forward (sub-cycled with respect to the larger time step of the implicit thermo-mechanical simulation), the RADAR models grid was kept much finer than the rest of the model, to reduce error, when linear projection was used to transfer the scaled volumetric power from RADAR to the rest of the model. The fuel burn-up serves as an important parameter for fission gas generation, fuel swelling and the changes in fuel thermal conductivity.

2.3 Pellet fracture model

Whilst most fuel behaviour can be accurately captured by 2D models, there are many features that require a full 3D model. One very important feature is the pellet cracking, which has two strong effects: one is fragment relocation and the other is an effect of the relaxation of the stresses and strains within each fragment [28]. The stresses within intact pellets and a cracked pellet can vary greatly [29]. Most axisymmetric models consider thermal loading comparable to those found within reactor. Therefore it is important that the model accounts for fragmentation and relocation as these effects will reduce the time to pellet cladding contact [30]. Some attempts have been made to model fracture in 3D pellets using cohesive zones to understand the pellets fractured stress state [31]. The relocation of pellet segments can be treated empirically and the relaxation of stresses can be treated through a modification of the material mechanical laws. Stress relaxation effects have been implemented in this model by the modification of the materials characteristics. Two different implementations of the material modification can be made: the material is treated as isotropic but with modified material properties or by replacing the material law with an anisotropic material model. The isotropic case proposed by Jankus and Weeks [32] was to consider an isotropic material where both the Young's modulus and the Poisson's ratio of the cracked material have been changed assuming the cracks were perpendicular to the fuel axis. The modified Young's modulus (E^c) and Poisson's ratio (ν^c) can be found from equations 2.5 and 2.6 where N is the number of cracks.

$$E^c = E \left(\frac{2}{3} \right)^N \quad 2.5$$

$$\nu^c = \nu \left(\frac{1}{2} \right)^N \quad 2.6$$

This modified isotropic behaviour was selected for its simplicity, and also permits modifications to allow cracked fuel to creep faster (see equation 2.7 where m is the stress exponent from the thermal creep, $\dot{\epsilon}_p$ is the equivalent plastic strain rate).

$$\dot{\epsilon}_p^c = \dot{\epsilon}_p \left(\frac{3}{2} \right)^{N(m-1)} \quad 2.7$$

2.4 Fission gas release

In a similar approach to [12] the fuel pin is treated as a fluid filled capsule, where the temperature of the fluid is determined by the average fuel surface temperature. The fluid within the pin changes with time and is modified from a user supplied sub-routine. The sub-routine computes the current thermal profile of the fuel and a Booth diffusion step is performed on virtual spherical grains [33]. The amount of fission gas released from a single grain for a particular radial distance is computed and repeated for every material point in the fuel. The value found is then integrated over the entire volume of the fuel and the fission gas released is added to the filling gas (See Fig. 4). The filling gas is treated as a mixture of helium, xenon and krypton. The thermal profile of the fuel and fuel surface temperatures are extracted from the FE simulation, the average of the fuel surface temperature was used [34]. This simple thermal model coupled to a fission gas diffusion model embedded within an ABAQUS routine shows the extensibility of ABAQUS and permits ever more accurate simulation of nuclear fuel.

More complex fission gas models have also been implemented with this model. These are capable of approximating diffusion of fission gas in the grains; trapping of gas at the grain boundaries; trapping in bubbles and simultaneously modelling the diffusion of the bubbles. This was accomplished by the use of a 1D FE model solving the coupled intragranular grain atom diffusion and bubble diffusion partial differential equations (of the form of equations 2.8 and 2.9) outlined in [35]. It is assumed these equations can be coupled by the fuels trapping and resolution parameters (implemented in TRANURANUS). This 1D FE model is solved at all fuel material points to approximate the total fission gas generation and release rate. This shows that an ABAQUS fuel performance code may incorporate multiple length scales, and an arbitrary number of models can be evaluated at all material points.

$$\frac{\partial C_s}{\partial t} = D_s \nabla^2 C_s - g C_s + b C_b + \beta \quad 2.8$$

$$\frac{\partial C_b}{\partial t} = g C_s - b C_b + D_b \nabla^2 C_b \quad 2.9$$

Where C_s and C_b are the in-solution gas concentration and the concentration of bubbles respectively. The parameters that govern motion are the diffusion coefficients D_s and D_b for atoms in solution and bubbles, g , b and β are the gas trapping, resolution and gas generation parameters respectively. Using the heterogeneous model for resolution, and that the trapping rate is diffusion controlled, with a dilute trapping density, the values for all fission gas release models parameters used in this study were computed from equations 3-6 in [35]. In the model outlined by van Uffelen et al. [35] insights from molecular dynamics studies were used to study the resolution parameter, making the implementation of this fission gas release model a multiscale enhancement for a FE fuel performance code.

2.5 Fuel and cladding material properties

The UO₂ fuel thermal behaviour is outlined in Table 2, showing the great number of non-linearities to be modelled by ABAQUS in the processes of simulating whole pin life. Table 3 shows many of the mechanical properties of the cladding, accounting for non-linear effects such as swelling, also included is a breakdown of how fuel creep was modelled.

A model to describe the fuel mechanical behaviour during power ramps is now presented. These mechanical properties are descriptive of the fuel elastic properties and its creep and swelling as a consequence the fuel in this model can be considered a visco-plastic material. The material properties for the visco-plastic behaviour of the fuel were extracted from the MATPRO

Material Library [36] that account for radiation induced; high stress and low stress creep (as defined in Table 2) with temperature and irradiation dependence.

3.0 Results and discussion

3.1 Thermomechanics

Fig. 5 shows a power ramp of new fuel from a shutdown state to 150% volumetric power. This ramp is designed purely to demonstrate the present modelling developments and is not representative of normal AGR operation. The cladding elongates to accommodate the increase in size of the fuel pellets due to thermal expansion. Despite small local plastically deformed regions forming around the locking pellet the extension of the whole fuel pin maintains a very close to linear relation of elongation to volumetric power. Local plastic strain in these locking regions is initially confined to several elements at the contact surface. On large ramps applied to the fuel the plastic region extends to the cladding outer surface.

Figs 6 and 7 characterise thermal behaviour of the fuel during heat up and power ramping. Axial variation from 1D models arise from the ASG pellets and the cladding. Fig. 6 shows the impact of fuel burn-up on the fuel centreline temperature. The centre temperature increases approximately 130°C over fuel life. Fig. 7 shows five standard pellets separated between a pair of locking pellets; the locking region shows a reduction in fuel centreline temperature compared to a standard pellet as a consequence of a reduced fuel radius and greater contact pressure with the cladding. While there was an increase of 130°C in the fuel centreline temperature, over fuel life, a smaller increase of just 20°C was observed for the cladding. The fuel centreline temperature changes observed are mostly a consequence of the reduction in the thermal conductivity of the fuel due to fuel burn-up.

Fig. 8 shows the cladding radial displacements throughout the simulated fuel pellet life. The displacement plot shows that, in the specific instance modelled, the creep down of the cladding onto the fuel occurs at about 310 days (6 GWd/tU burn-up). The displacement of the cladding increases radially as the fuel swells after contact and clad creep down. The increase in stress in the cladding, induced by pellet swelling, develops too slowly with respect to the high cladding creep rate to permit the development of plastic strain under normal operating conditions. Therefore the large radial displacements observed in the cladding are produced from creep strain, confirming the source of cladding damage from long term normal operation is from creep damage/ductility exhaustion. The displacement plots show the cladding radial displacements. Contact of the pellet and cladding triple point, here we define a triple point as the region where two adjacent pellet ends intersect the cladding, as an initial sharp outward displacement and as the thermal expansion and swelling of the fuel continues the triple point increases its outward movement and the cladding is deformed about the pellets vertices.

At the very start of life a 30 micron expansion of the cladding occurs. This is due to the pre-heating of the reactor core to 350°C. This fuel pin pre-heating causes the filling gas (ideal gas) to expand. There is also an over prediction of the gas temperature as the gas takes on the temperature consistent with the pellets centreline temperature. Also as the fuel begins heat generation the cladding thermally expands with an expansion of over twice that of the fuel. It is noted that there is an initial condition sensitivity, with regards to the selected gas temperature, as to when the cladding has completely collapsed on to the pellets.

3.2 Radial fuel rating

The behaviour of the fuel centre and the surface differ greatly, this radial difference is primarily a consequence of the variation in radial power. This power difference arises from a neutron flux difference leading to fissionable material distribution differences. To characterise this Fig. 9 shows the power at 5 positions on the pellets radius: 1, 0.875, 0.75, 0.5, 0 (normalised pellet radius $\frac{r-r_0}{r_1-r_0}$ where r_0 and r_1 are the pellet inner and outer radii respectively). The volumetric power at the radial points show that the increase in plutonium at the pellet rim and its relatively slow diffusion from the surface can cause up to a 30% increase in the rims volumetric power generation. The increase in surface rating raises the surface temperature, despite direct contact with the cladding acting as a heat sink. This elevated temperature potentially accelerates any corrosion or bonding processes occurring at the claddings inner surface. These strong dynamics at pellet surfaces make power considerations essential in PCI behaviour modelling.

3.3 Fission gas model

The fission gas is modelled as an ideal gas in a volume that's size is linked to the mechanical deformation of the cladding and the central hole. The pressure increase in the AGR fuel is presented in Fig. 10 and is less than that of a light water reactor fuel. This lower pressure is due to the annular fuel geometry, the central hole does not suffer any significant reduction in size, from fuel expansion and swelling, for the modelled five years of reactor time. The central hole contains all of the fission gas when the pellet cladding gap closes. In principle as the fuel ages the migration of fission gas, will alter the pellet geometry, however this is not considered in the current model.

3.4 Cladding

3.4.1 End caps

The AGR fuel pin geometry does not undergo substantial volume change under the current modelling conditions. The point which undergoes the greatest displacement under the 'normal' operating conditions is the unconstrained end cap centre. The end cap centre sees a displacement inwards by about 2 mm as the reactor reaches its operating pressure. As the pins internal pressure increases the end cap is displaced outward again. By the end of a 5 year dwell time in the reactor the internal pressure is still not sufficient to overcome the external pressure from the coolant, this is in agreement with a typical design constraint for over-gassing in fuel, the lower AGR coolant pressure makes this a fuel life limiting factor (see, Fig. 11).

3.4.2 Anti-stacking groove

The impact of the ASG locking region can be seen in Fig. 12, which shows the von Mises stresses after a heat-up (A), the plastic strains after a heat-up to full power (B) and the plastic strains after a power ramp to 150% (C). Although several locking geometries were modelled only one is shown. All modelled geometries exhibited pellet contact throughout life. All geometries modelled also exhibited local yielding on the initial heat up of the fuel pin. In all of the locking geometries two areas experienced the highest von Mises stresses of about 325 MPa. These areas are the bottom of the locking region, as defined by the closest end of the lock to fuel centre, and

the middle of the locking region. The few models, run at 100% power, where there was cladding through thickness yielding in the locking section, the plastic strains were at a maximum at the end of the locking regions (9.6×10^{-4}). This very high value was strongly dependent on the spacer pellet region. i.e. the inclusion of a half standard pellet, between the spacer pellet and locking pellet, would reduce this strain. When compared with the next inner locking region there is an order of magnitude drop in plastic strain. There was little difference in the stress states shown in the locking section in the case of bonded and unbonded simulations. The relatively high friction for the unbonded case and the normal direction pressure induced by the coolant ensured that the cladding inner surface and fuel outer surface displace together with very little sliding. This locking region of the fuel pin remains in contact for the whole simulation; this remains the case in both the bonded and unbonded simulations for the full range of tested powers, inclusive of late life cool downs due to swelling. As the locking surfaces do not separate (significantly) during the simulation the surfaces were tied. While tying the surfaces does not significantly alter the results the number of increments to a complete simulation was greatly reduced.

Fig. 13 shows a asymmetry in the equivalent plastic strain contour in the case of the unbonded model. This asymmetry in the location of the plastic region may originate from slipping of contact surfaces at the pellet cladding triple point before the complete axial expansion of the fuel within the cladding occurs. In the bonded case this asymmetry is greatly reduced as once contact is made the motion of the cladding inner surface will match the motion of the pellet. While for the locking region the bonding between the fuel and the cladding may not be very significant at the triple point, bonding and a power ramp forms a significant plastic region through the cladding. This through cladding yielding would reduce the ductility at any pellet-cladding interfaces. Considering radial cracks this would produce networks of plastic regions, which combined with irradiation damage (in cladding He production) and loss of ductility through creep are potential areas of failure.

3.4.3 Alumina spacer pellet influence

The alumina spacer pellet is shown as the half height pellet just above the pin end cap in Fig. 1. The constant heat up and cooling of the fuel may cause wear on the welded end caps, alumina has previously served as tube liners in abrasive environments and metallic component protection in other ceramic fuels [37]. This protection was achieved due to the high thermal conductivity and small thermal expansion of alumina. The spacer pellet is non-heat generating and therefore serves as thermal protection to the fuel pin ends. In all load cases the spacer pellet was able to protect the cladding and the weld points remained at coolant temperature. This is up to 50°C lower than the cladding temperature at the midsection of the fuel pin. As well as the reduced temperature in the cladding the stiffness of the spacer pellet, coupled with the fact the fuel pellet adjacent to it is an ASG pellet, has led to reduced stresses in the end cap region. This results in an equivalent plastic strain of 2.5×10^{-4} even after a power spike to 150% power. The combination of reduced stress and temperature in the cladding has also reduced the creep strain surrounding the spacer pellet reducing the risk of damage to the end cap welds from creep ductility exhaustion.

The spacer pellet also limits the region of plastic deformation at the end caps to several surface elements. This suggests yielding here is a consequence of spacer pellet friction with the cladding. The plastic strain is more than an order of magnitude less than all other plastic regions

in the fuel pin. Without the spacer pellet the weld is expected to experience significant creep and plastic deformation leading to very rapid degradation of the fuel pins ability to contain fission products. The von Mises stress, creep and plastic strain can be seen in Fig. 14. The most significant region of creep and plastic strain in the end caps results from the friction between cladding and pellet and the geometry of the spacer, which places the region of significant plastic strain (0.1%) at the intersection of the spacer pellets and the cladding (point a in Fig. 14).

3.5 Information management

The very large quantity of information that is produced from a single run of a whole pin, over a whole life model, leads to a situation where it may be difficult to discern behaviour of the fuel as a function of load history. There exists a very powerful indicator as to the condition of the fuel (thermally and mechanically) in the value of the thermal conductivity plotted as a function of time/burn-up (See, Fig. 15a). The thermal conductivity links almost all aspects of fuel behaviour. It controls the fuel thermal profile, influencing its expansion and swelling, leading to mechanical working of the cladding. The thermal conductivity has strong non-linear temperature dependence (see, Fig. 15b). As the fuel expands and the fuel cladding gap closes, the thermal profile responds to the change in the heat transfer coefficient of the gap, the change in thermal profile would need to equilibrate with the thermal conductivity to reach steady state. The thermal conductivity also responds to chemical changes, this can be from material change as a consequence of reactor dwell or changes in the fuel's heat generating state (local rating differences). It would decrease as the fuel burns up and responds due to rating changes, increasing or decreasing as fissile material is destroyed or created respectively.

Fig. 15a shows that the behaviour of the fuel can be described from analysis of a single material property change. Following through life we find: Point A shows the initial fuel heat up. Here, the centreline temperature increases with respect to the fuel surface temperature and therefore the thermal conductivity reduces in the pellet centre by about 10%. Point B shows the period when the cladding creeps down and the gap size is similar to the mean free path length of the filling gas. At this time the fuel surface temperature increases and the thermal conductivity responds by decreasing. Point C is when clad creep down is complete and the start of the fuel power spike and cycling begins. Point D is long term operation where the increase in burn-up adversely affects the fuel centre and surface thermal conductivity. Point E is the finish of the stabilisation of the plutonium generation and diffusion and with full cladding contact the surface temperature can stabilise. The steady decline of both the surface and the centreline thermal conductivity correspond to the continual burn-up of the fuel while the fuel is in reactor. Fig. 14b. shows the proposed thermal conductivity from reference [34]. Table 1 shows the different contribution to the thermal conductivity. The properties are collected in such a way that each contributing factor may be independently modelled, perhaps even on different length scales.

4.0 Conclusions

The implementation of a nuclear fuel performance code into a commercial FE package is becoming more common place as the capabilities and performance of general FE packages continue to improve. The benefits in a fuel performance code are:

- The usability of a FE based fuel performance code would be an enhancement over past codes.

- Pre- and post-processors have lowered the entry barrier for the development of a fuel performance model to permit the ability to model complicated systems.
- Typical runtimes for a 5 year axisymmetric model takes less than one hour on a single core workstation.

The current model has implemented:

- Non-linear fuel thermal behaviour, including a complex description of heat flow in the fuel. Coupled with a variety of different FE and finite difference models.
- Non-linear mechanical behaviour of the fuel and cladding including, fuel creep and swelling and cladding creep and plasticity each with dependencies on a variety of different properties.
- A fission gas release model which takes inputs from first principles calculations.
- Explicitly integrated inventory calculations performed in a coupled manner.
- Freedom to model steady state and transient behaviour using implicit time integration.
- The whole pin geometry is considered over an entire typical fuel life.

The model showed by examination of normal operation and a subsequent transient chosen for software demonstration purposes:

- ABAQUS may be a sufficiently flexible platform to develop a complete and verified fuel performance code.
- The importance and effectiveness of the geometry of the fuel spacer pellets was characterised.
- The fuels performance under normal conditions (high friction no power spikes) would not suggest serious degradation of the cladding in fuel life.
- Large plastic strains were found when pellet bonding was strong, these would appear at all pellets cladding triple points and all pellet radial crack and cladding interfaces thus showing a possible axial direction to cracks forming from ductility exhaustion.

Acknowledgements

One of the authors (R Mella) wishes to thank EPSRC for funding through a departmental training account. Both authors wish to thank the Fuels Group at EDF energy, Barnwood, Gloucester, for both financial support and discussions. However, the views expressed here represent those of the authors and not necessarily those of EDF Energy.

References

- [1] F. Bentejac, N. Hourdequin, in:., Pellet-clad Interaction in Water Reactor Fuels, Aix-en-Provence, France, 2004, pp. 495–506.

- [2] B. Michel, J. Sercombe, G. Thouvenin, Nucl. Eng. Des. 238 (2008) 1612.
- [3] B. Michel, J. Sercombe, G. Thouvenin, R. Chatelet, Eng. Fract. Mech. 75 (2008) 3581.
- [4] C. Struzik, D. Plancq, B. Michel, P. Garcia, C. Nonon, in: Pellet-clad Interaction in Water Reactor Fuels, Aix-en-Provence, France, 2004, pp. 507–517.
- [5] M. Valach, J. Zymak, in: Pellet-clad Interaction in Water Reactor Fuels, Aix-en-Provence, France, 2004, pp. 441–451.
- [6] S.P. Walker, R.T. Fenner, Nucl. Eng. Des. 138 (1992) 403.
- [7] A. Yu, S.P. Walker, R.T. Fenner, Nucl. Eng. Des. 121 (1990) 53.
- [8] G. Zhou, J.E. Lindbäck, H.C. Schutte, L.O. Jernkvist, A.R. Massih, in: Pellet-clad Interaction in Water Reactor Fuels, Aix-en-Provence, France, 2004, pp. 519–530.
- [9] J.-S. Cheon, Y.-H. Koo, B.-H. Lee, J.-Y. Oh, D.-S. Sohn, in: Pellet-clad Interaction in Water Reactor Fuels, OECD, Aix-en-Provence, France, 2004, pp. 191–201.
- [10] V. Guicheret-Retel, F. Trivaudey, M.L. Boubakar, R. Masson, P. Thevenin, in: Pellet-clad Interaction in Water Reactor Fuels, Aix-en-Provence, France, 2004, pp. 453–463.
- [11] N. Marchal, C. Campos, C. Garnier, Comp. Mater. Sci. 45 (2009) 821.
- [12] R.L. Williamson, J. Nucl. Mater. 415 (2011) 74.
- [13] R.L. Williamson, J.D. Hales, S.R. Novascone, M.R. Tonks, D.R. Gaston, C.J. Permann, D. Andrs, R.C. Martineau, J. Nucl. Mater. 423 (2012) 149.
- [14] H.S. Aybar, P. Ortego, Prog. Nucl. Energ. 46 (2005) 127.
- [15] G.A. Berna, C.E. Beyer, K.L. Davis, D.D. Lanning, FRAPCON-3: A Computer Code for the Calculation of Steady-State, Thermal-Mechanical Behavior of Oxide Fuel Rods for High Burn-up, Idaho National Engineering and Environmental Laboratory, NUREG/CR-6534, n.d.
- [16] K.J. Geelhood, W.G. Luscher, C.E. Beyer, J.M. Cuta, FRAPTRAN 1.4: A Computer Code for the Transient Analysis of Oxide Fuel Rods, NUREG/CR-7023, 2011.
- [17] K. Lassmann, J. Nucl. Mater. 188 (1992) 295.
- [18] EDF Energy, The ENIGMA Fuel Performance Code Description: Version 5.14, n.d.
- [19] J.C. Killeen, J.A. Turnbull, E. Sartori, in: International LWR Fuel Performance Meeting, 2007, p. 1102.
- [20] EDF Energy, Private Communications (2011).
- [21] ABAQUS Software, Rising Sun Mills, 166 Valley Street, Providence, RI. (2011).

- [22] D.L. Olander, *Fundamental Aspects of Nuclear Reactor Fuel Elements*, 1978.
- [23] K. Lassmann, F. Hohlefeld, *Nucl. Eng. Des.* 103 (1987) 215.
- [24] A.M. Ross, R.L. Stoute, *Heat Transfer Coefficient Between UO₂ and Zircaloy-2*, Canadian Report AECL-1552, 1962.
- [25] A.L. Lindsay, L.A. Bromley, *Ind. and Eng. Chem.* 42 (1950) 1508.
- [26] P. Van Uffelen, R.J.M. Konings, C. Vitanza, J. Tulenko, *Handbook of Nuclear Engineering: Nuclear Engineering Fundamentals*, 2010.
- [27] I. Palmer, K. Hesketh, P. Jackson, *Water Reactor Fuel Element Performance Computer Modelling.*, 1983.
- [28] K. Lassmann, H. Blank, *Nucl. Eng. Des.* 106 (1988) 291.
- [29] G.P. Mezzi, F. Caligara, H. Blank, *Nucl. Eng. Des.* 73 (1982) 83.
- [30] T. Helfer, P. Garcia, J.-M. Ricaud, D. Plancq, C. Struzik, in: *Pellet-clad Interaction in Water Reactor Fuels*, Aix-en-Provence, France, 2004, pp. 367–377.
- [31] R.L. Williamson, D.A. Knoll, in: *20th International Conference on Structural Mechanics in Reactor Technology (SMIRT 20)*, Espoo (Helsinki), Finland, 2009, p. 1775.
- [32] V.Z. Jankus, R.. Weeks, *Nucl. Eng. Des.* 18 (1972) 83.
- [33] J.A. Turnbull, C.E. Bayer, *Background and Derivation of ANS-5.4 Standard Fission Product Release Model*, NUREG/CR-7003, 2010.
- [34] P.G. Lucuta, H. Matzke, I.J. Hastings, *J. Nucl. Mater.* 232 (1996) 166.
- [35] P. Van Uffelen, G. Pastore, V. Di Marcello, L. Luzzi, *Nuc Eng. and Tech.* 43 (2011) 477.
- [36] C.M. Allison, *SCDAP/RELAP5/MOD3.1 Code Manual. Volume IV: MATPRO*, Idaho National Engineering Laboratory Technical Report, NUREG/CR-6150, 1993.
- [37] J. Rouault, P. Chellapandi, B. Raj, P. Dufour, *Handbook of Nuclear Engineering: Nuclear Engineering Fundamentals*, 2010.

Figure captions

Fig. 1: (a) Quarter section of a pin end showing half height spacer pellet (bottom) and cladding locking into an ASG pellet (second bottom). (b) An ASG pellet, (c) a conventional annular fuel pellet. Image depicts the end of the fuel pin showing the end stand and the welded in end caps.

Fig. 2: Meshes of axisymmetric pellet segments; A) Spacer pellet mesh and the end cap; b) central region of an ASG pellet and surrounding cladding; (c) Interface between two pellets.

Fig. 3: Typical amplitude curve for heat up, long term steady operation and end of life ramping and cycling. This figure shows the three domains of particular interest. (A) One week heat up to 100%. (B) Power profile of power spike at one year dwell time. (C) A short online refuelling cycle. (C) Flat profile for the rest of life.

Fig. 4: Procedure executed within USDFLD subroutine, within ABAQUS to approximate the increase in pressure within the fuel central hole.

Fig. 5: Computed pin elongation, from the centre of pin, for heat-up from zero power to different values of volumetric power.

Fig. 6: Plot of the impact of fuel burn-up on the fuel centreline temperature. The figure shows the fuels thermal profile at start of life and thermal profile at end of five year operation at 100% power. While there is a change in thermal profile from the pellet cladding gap closing the greatest difference in centreline temperature is from fuel material non-linearity.

Fig. 7: Axial thermal centreline profile of a segment of AGR fuel. Each segment is 5 pellets enclosed at each end with an ASG pellet.

Fig. 8: shows the cladding radial displacements throughout the simulated fuel pellet life. The plot of displacement is for a section of cladding over several standard fuel pellets. The displacement plot shows that the creep down of the cladding on to the fuel occurs at about 6GWd/tU. The plot shows the bamboo pin shape expected with pelleted fuel.

Fig. 9: The volumetric power of a fuel pellet near the centre of the pin at different pellet radii, the radii that correspond to A, B, C, D and E correspond to 1, 0.875, 0.75, 0.5, 0 from the surface in units of pellet radius.

Fig. 10: Shown is the internal pin pressure, volume change due to fission gas and the average fission gas release fraction for the AGR as a function of fuel burn-up. The fraction axis have normalised units. The normalised units are defined as $V-V_f/V_i-V_f$ for volume where the i and the f subscripts stand for initial and final respectively. Similarly for pressure, $P-P_f/P_i-P_f$, where the i and the f subscripts stand for initial and final respectively.

Fig. 11: Point of greatest displacement due to end cap doming as a result of fission gas release and fuel expansion as a function of burn-up. Negative displacement defined as inward end cap doming.

Fig. 12: (A) The von Mises stress (Pa) on a typical locking region after a heat-up to full power of 125 MW/m³, circled regions are points of highest stress. (B) Equivalent plastic deformation after a typical heat-up to full power, still holding much of its symmetry. (C) Equivalent plastic deformation at end of life after power spike to 150% full power of 187.5 MW/m³.

Fig. 13: (A), (B) and (C) show the plastic region at the triple point between cladding and two separate pellets for the unbonded case, they show the plastic region at three different points, after heat-up, while power spike is in progress and at the end of the power spike respectively.

(D), (E) and (F) show the plastic region at the same triple point between cladding and two separate pellets for the bonded case for the same cases as (A), (B) and (C).

Fig. 14: (A), (B) and (C) show the protective effect of the spacer pellet on the pin end caps, they show the von Mises stress (Pa), equivalent creep strain and the equivalent plastic strain at the end of life. The figure only shows a cross section of cladding end with the axisymmetric model rotated by 180°. The fuel and spacer pellets have been removed to show clearly the cladding stress state.

Fig. 15a: The thermal conductivity of a standard pellet near the centre of the pin throughout life. Shown is the fuel centreline and fuel surface thermal conductivity. 15b: The thermal conductivity profile as a function of temperature and burn-up proposed by Lucuta et al. [33].

Table 1: Model run parameters.

Property	Value
Volumetric Body Flux (MW m^{-3})	125
Fast Neutron Flux ($\text{n m}^{-2} \text{s}^{-1}$)	4×10^{17}
Coolant Pressure (MPa)	4
Coolant Outlet Temperature ($^{\circ}\text{C}$)	650
Pin Filling Gas	Helium
Fill Gas Initial Pressure (MPa)	0.1
Fuel Surface Roughness (10^{-6}m)	3
Clad Surface Roughness (10^{-6}m)	2
Fuel Emissivity	0.88
Clad Emissivity	0.8
Clad Hardness (GPa)	1
Pellet-Clad Coefficient of Friction	0.8
Number of Pellet Cracks	5

Table 2: Fuel material properties and their associated parameters.

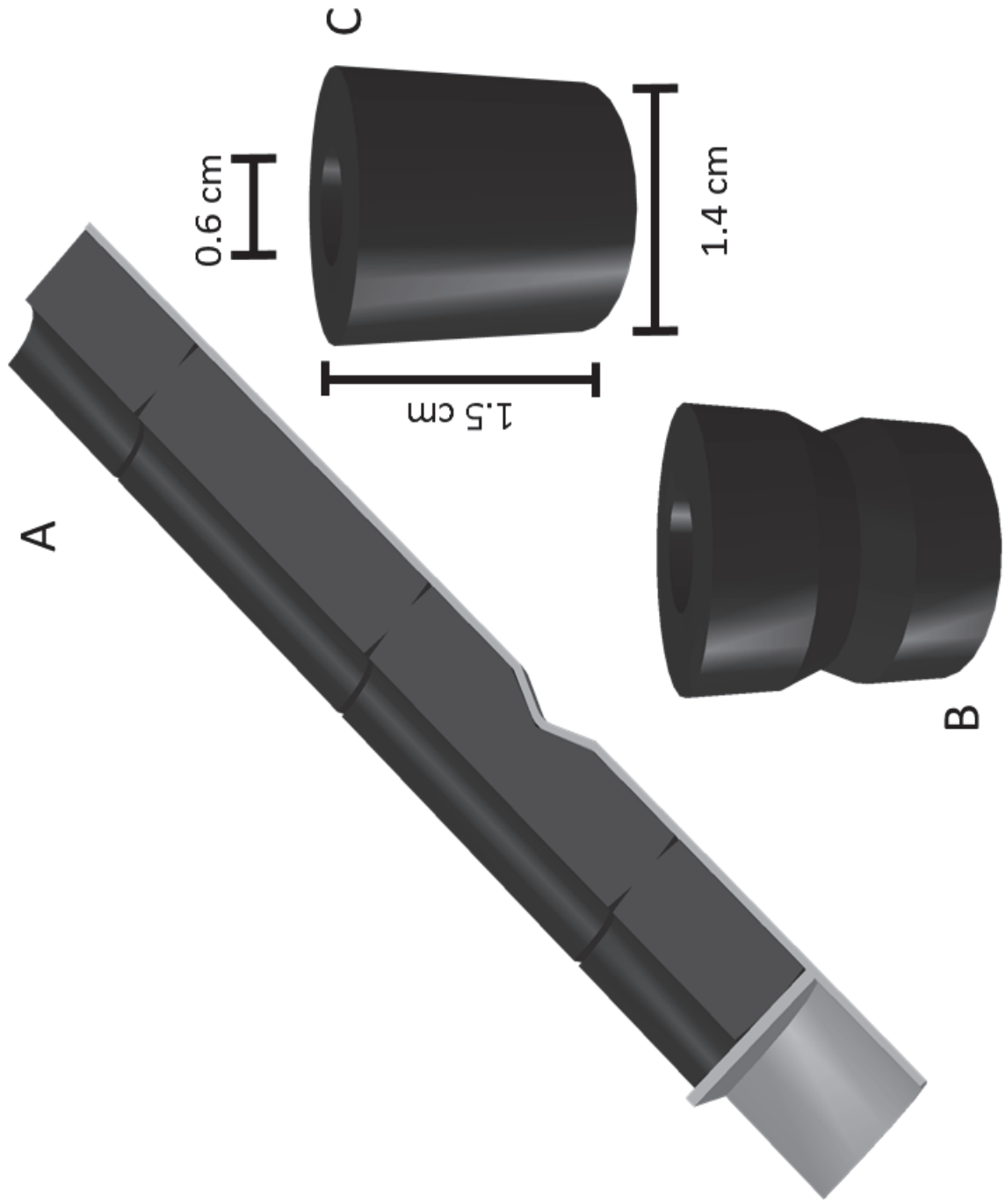
Property	Symbol	Units	Form	Parameters	Source
Thermal Conductivity	λ	$\text{W m}^{-1} \text{K}^{-1}$	$k_1(\beta)k_2(p)k_3(x)k_4(r)\lambda_0(T)$	See Source	[33]
Specific Heat Capacity	c_p	$\text{J Kg}^{-1} \text{K}^{-1}$	$k_a + k_b(T - 293)$	$k_a = 0.257$ $k_b = 5. \text{E} - 5$	[18]
Density	ρ	Kg m^{-3}	10690		[18]
Thermal Expansivity	α	K^{-1}	$Ex_a T + Ex_b T^2 + Ex_c T^3$	$Ex_a = 8.5524\text{E} - 6$ $Ex_b = 1.2793\text{E} - 9$ $Ex_c = 1.32\text{E} - 12$	[18]
Young's Modulus	E	MPa	1.94E5		[18]
Poisson's Ratio	ν	-	0.325		[18]
Total Creep Rate	$\dot{\epsilon}_{tot}$	s^{-1}	$\dot{\epsilon}_{tot} = \dot{\epsilon}_{low} + \dot{\epsilon}_{high} + \dot{\epsilon}_{irr}$		[18]
Low Stress Creep Rate	$\dot{\epsilon}_{low}$	s^{-1}	$\dot{\epsilon}_{low} = A_l \sigma^{n_l} e^{\frac{Q_l}{T}}$	$A_l = p_r 1.226\text{E}-7/\text{G}$ $n_l = 1.0$ $Q_l = 45220.0 \text{K}$	[18]
High Stress Creep Rate	$\dot{\epsilon}_{high}$	s^{-1}	$\dot{\epsilon}_{high} = A_h \sigma^{n_h} e^{\frac{Q_h}{T}}$	$A_h = p_r 8.8\text{E}3$ $n_h = 4.5$ $Q_h = 67110.0 \text{K}$	[18]
Irradiation Creep Rate	$\dot{\epsilon}_{irr}$	s^{-1}	$\dot{\epsilon}_{irr} = A_F \dot{F} \sigma^{n_i}$	$A_F = 1.4\text{E}-30$ $n_i = 1.0$	[18]
Fast Neutron Flux Rate	\dot{F}	$\text{N m}^{-2} \text{s}^{-1}$	4E15 (at 100% power)		
Solid Fission Product Swelling increment	$\Delta \epsilon_{sws}$	-	$\Delta \epsilon_{sws} = 6.407 \times 10^5 \rho \Delta Bu$		[36]

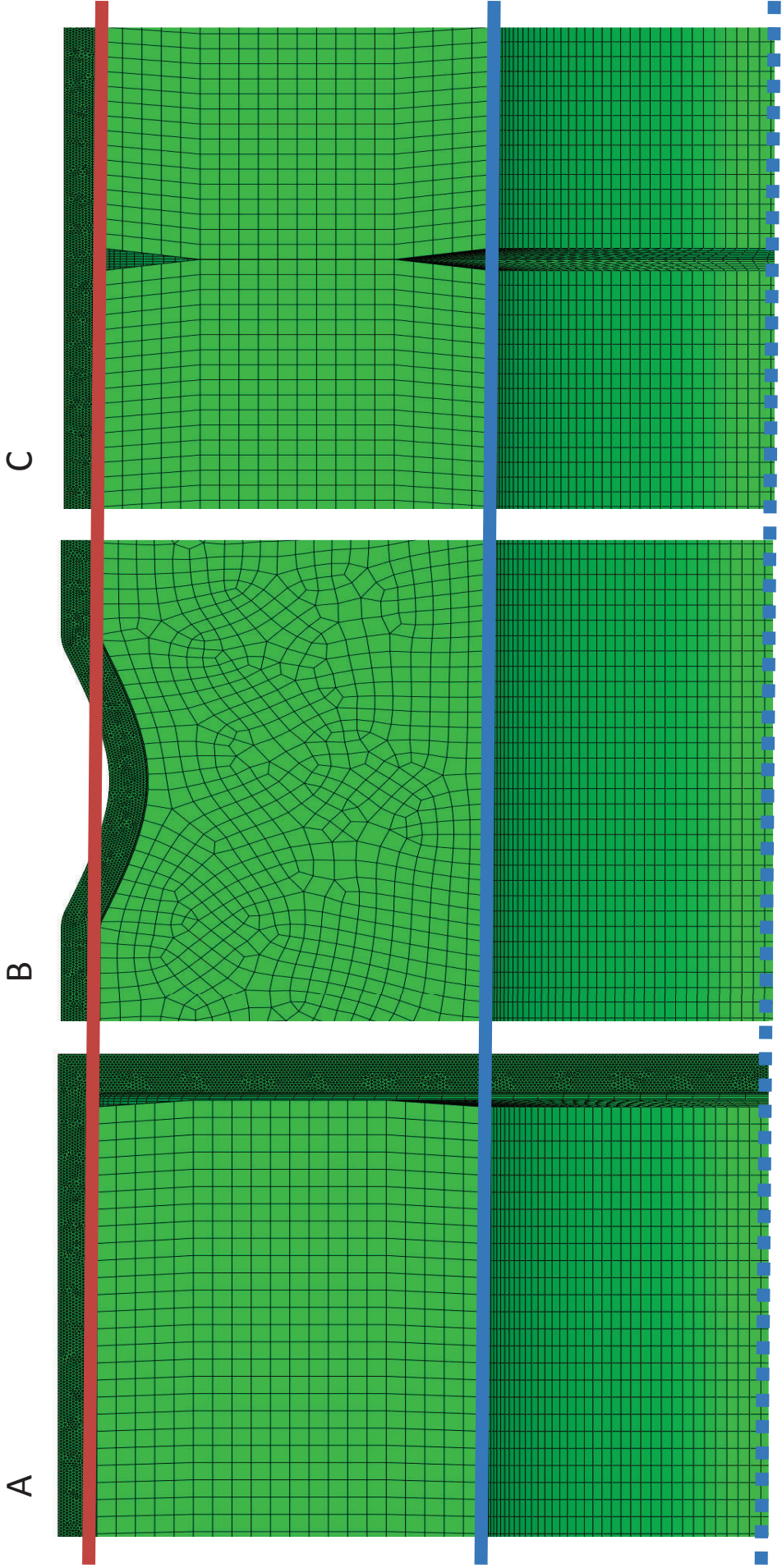
Gaseous Fission Product Swelling increment	$\Delta\varepsilon_{swg}$	-	$\Delta\varepsilon_{swg} = 2.25 \times 10^{-31} \rho$ $\Delta Bu(2800 - T)^{11.73} e^{-0.0162(2800 - T)}$ $e^{-0.021 \rho Bu}$	[36]
<p>All temperatures (T) are absolute temperature. <i>Bu</i> and ΔBu is the burn-up and burn-up increment respectively with units of %FIMA. Input G is the grain size in mils. p_r is the total fractional porosity as input from user.</p>				

Table 3: Stainless steel (25 wt% Ni, 20 wt% Cr, 0.05 wt% C and 0.5 wt% Nb) cladding material properties and their associated parameters.

Property	Sym	Units	Form	Parameters	Source
Thermal Conductivity	λ	$W m^{-1} K^{-1}$	$k_a + k_b T$	$k_a = 0.257$ $k_b = 5. E - 5$	[18]
Specific Heat Capacity	c_p	$J Kg^{-1} K^{-1}$	624		[18]
Density	ρ	$Kg m^{-3}$	8010		[18]
Thermal Expansivity	α	K^{-1}	$Ex_a T + Ex_b T^2 + Ex_c T^3$	$Ex_a = 1.436E - 5$ $Ex_b = 6.0E - 9$ $Ex_c = 0$	[18]
Young's Modulus	E	MPa	1.68E5		[18]
Poisson's Ratio	ν	-	0.3		[18]
Clad Creep Rate	$\dot{\varepsilon}_{clad}$	s^{-1}	$\dot{\varepsilon}_{clad} = A_1 \sigma^{n_1} e^{\frac{Q_1}{T}}$ $+ A_2 \sigma^{n_2} e^{\frac{Q_2}{T}}$ <p>For T > 400K</p>	$A_1 = 4.4856E7$ $n_1 = 1.724$ $Q_1 = 43801.0K$ $A_2 = 9.4257E - 3$ $n_2 = 5.8152$ $Q_2 = 34789.0K$	[18]

Figure

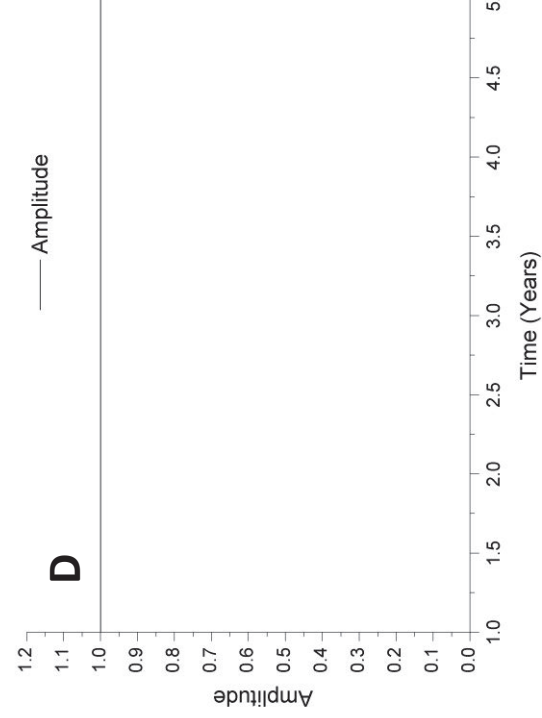
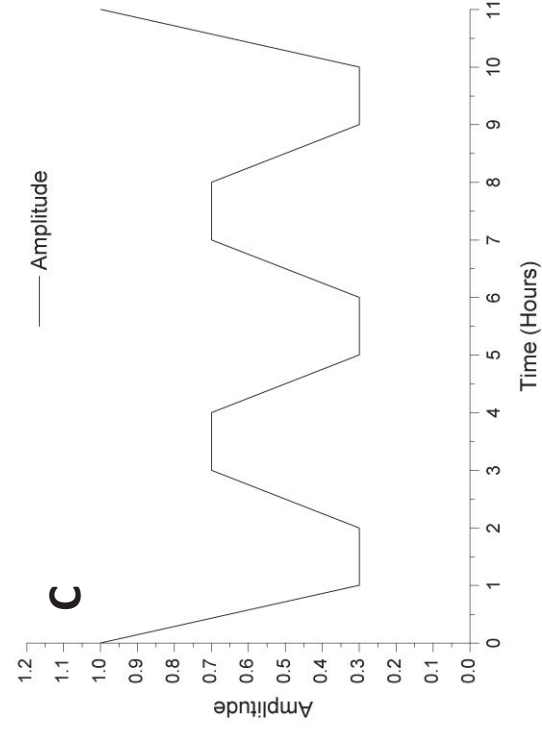
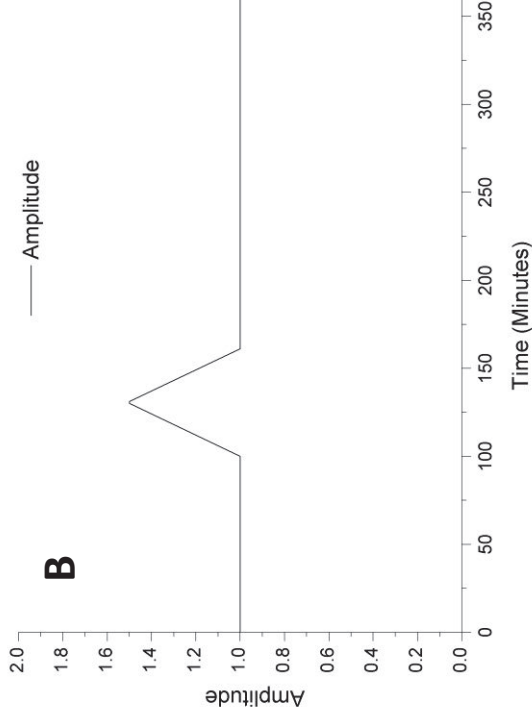
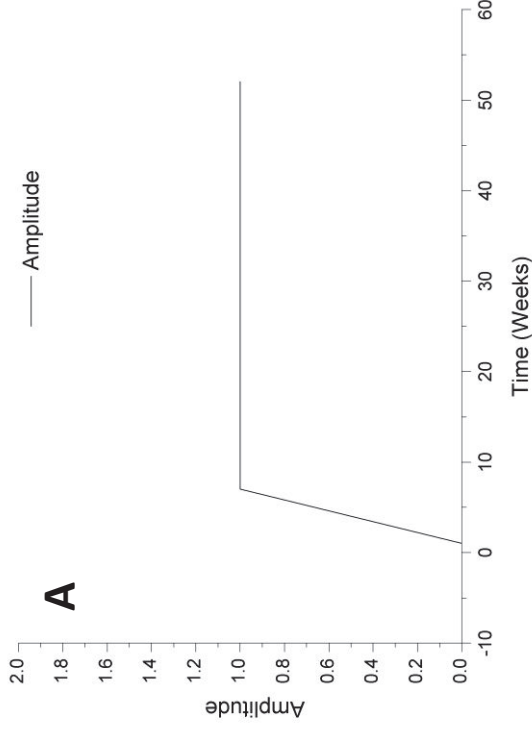


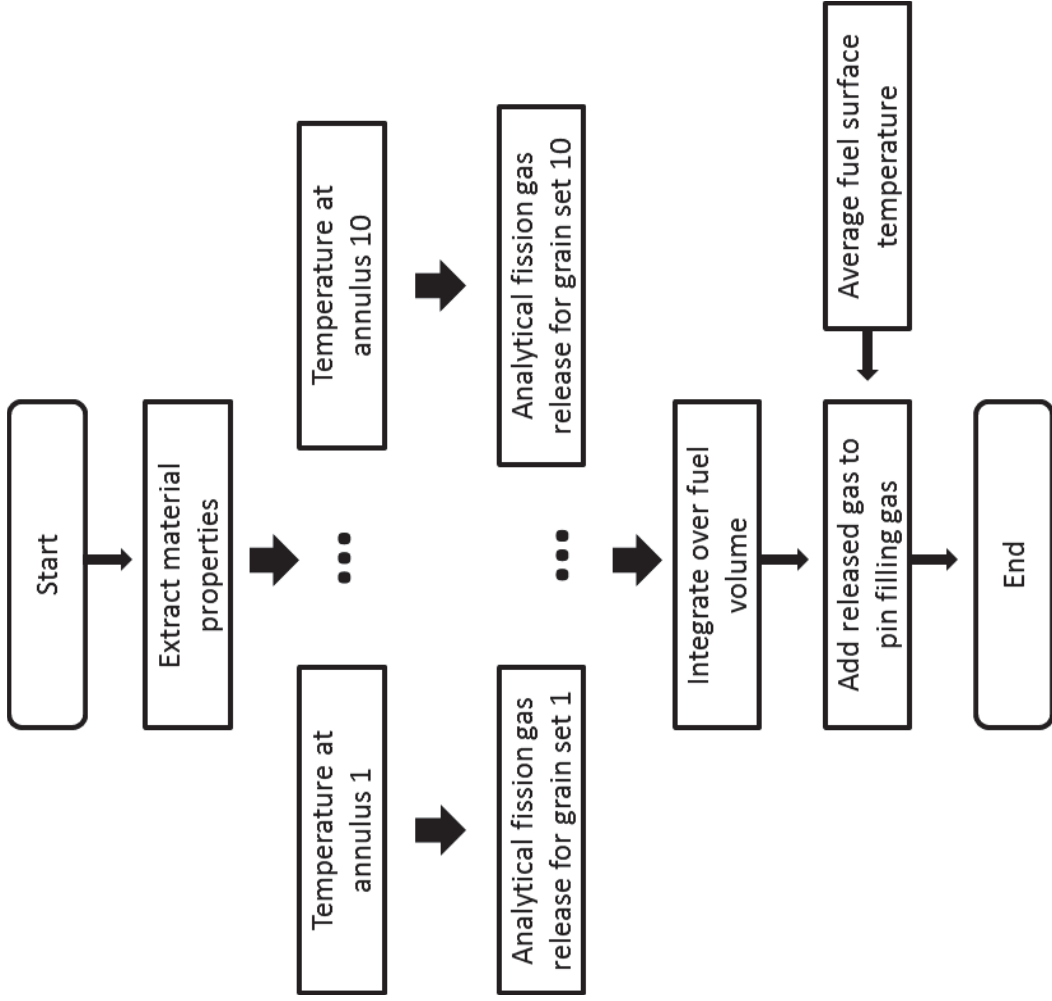


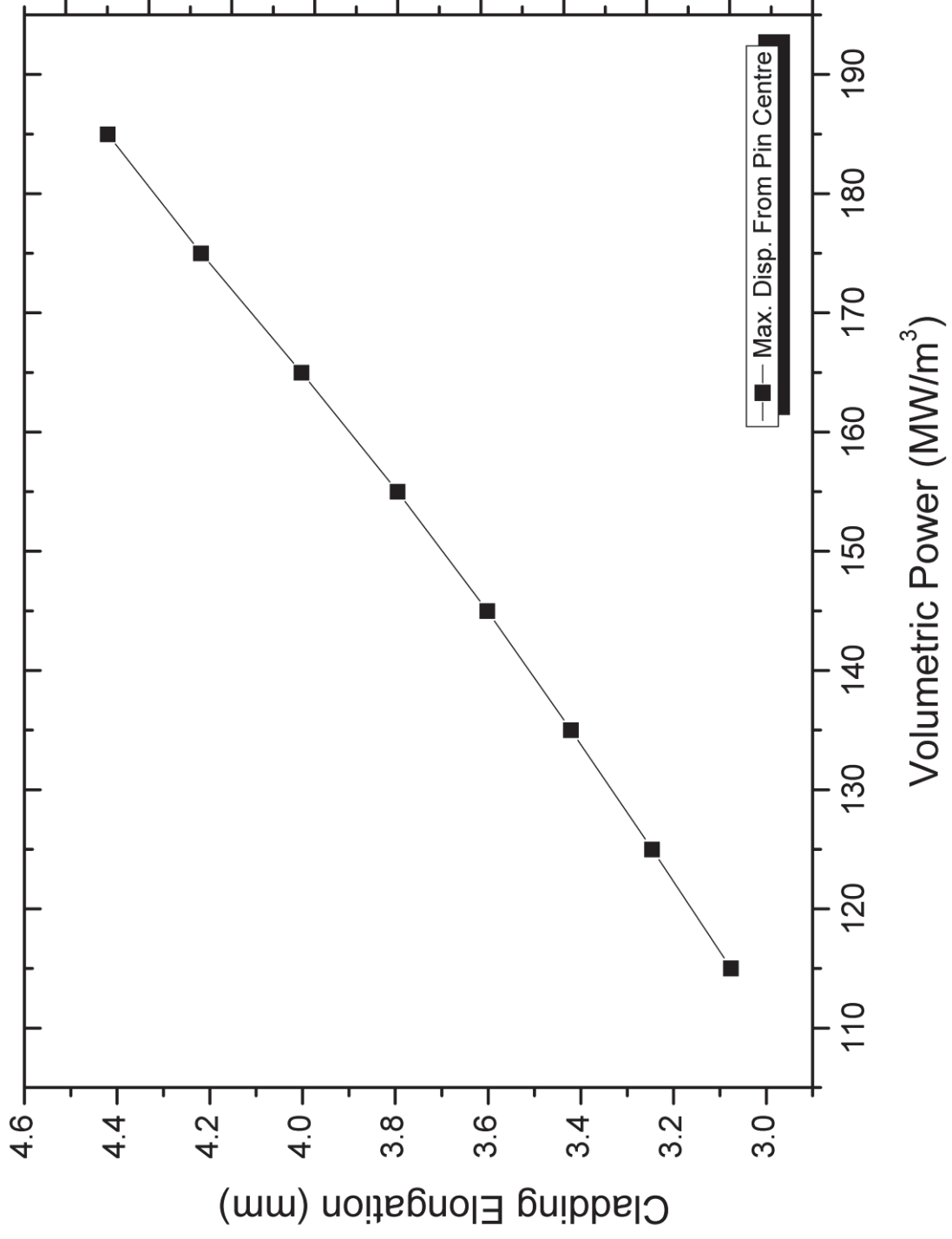
■ ■ ■ Centreline

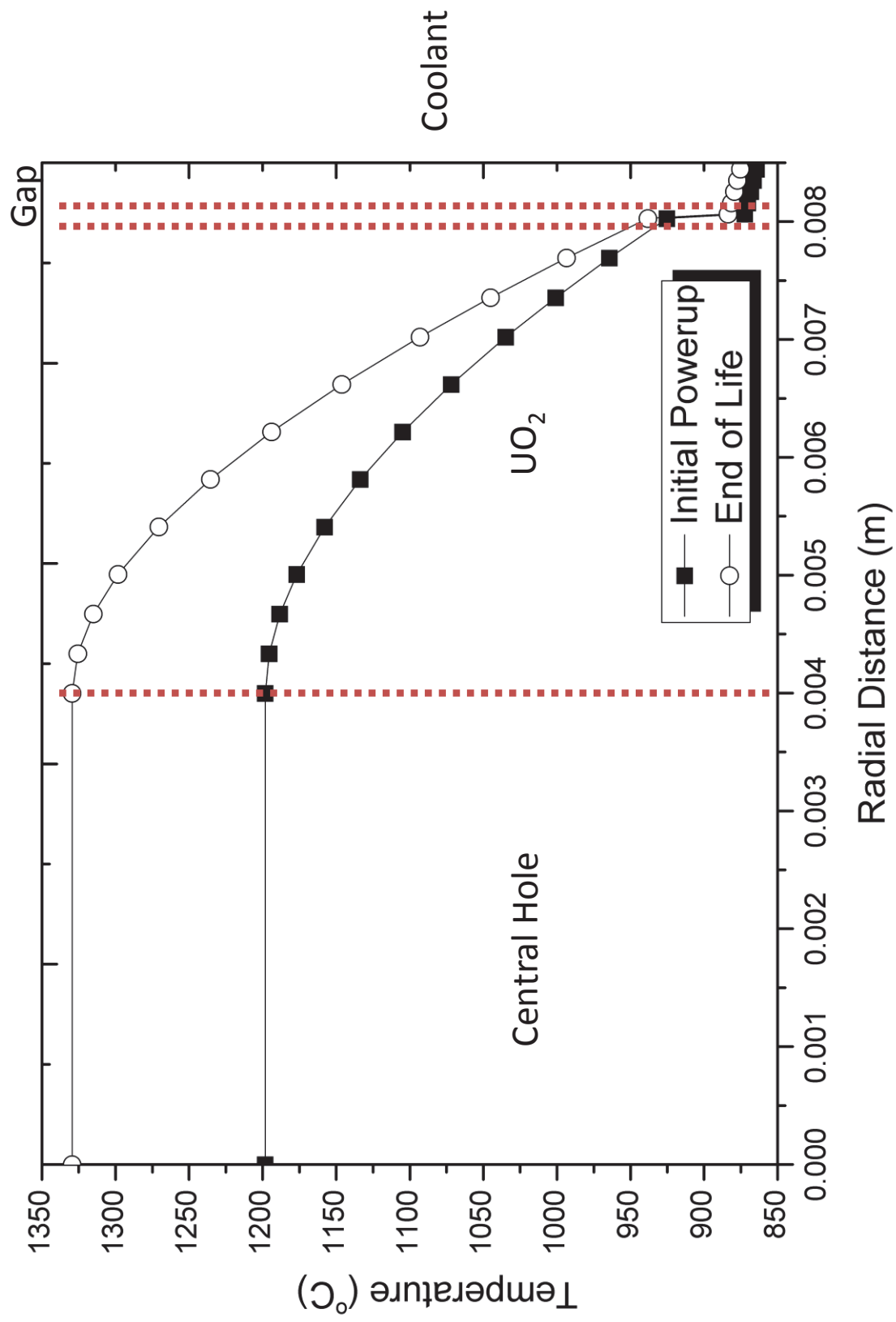
■ Inner Pellet Radius

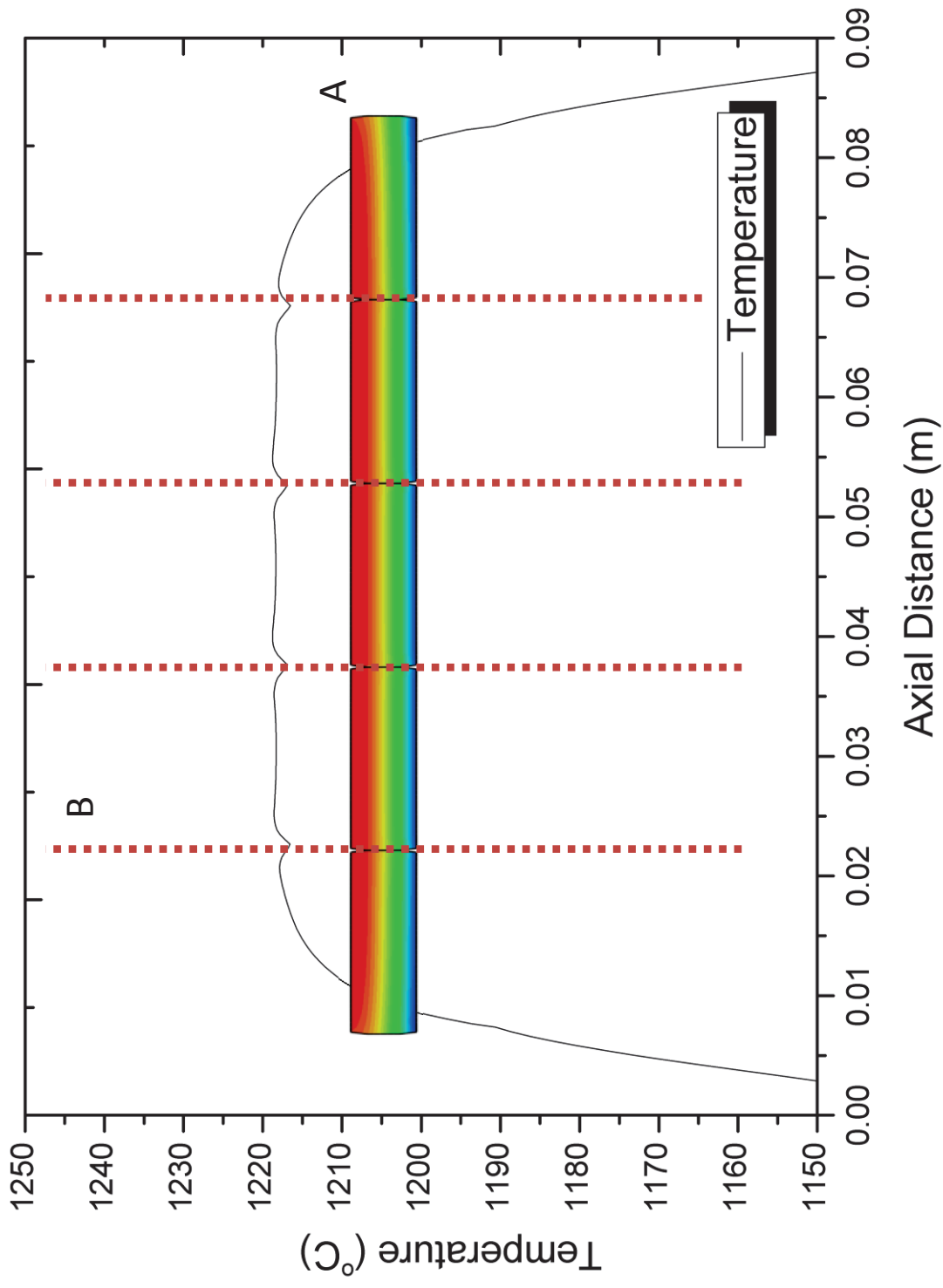
■ Outer Pellet Radius

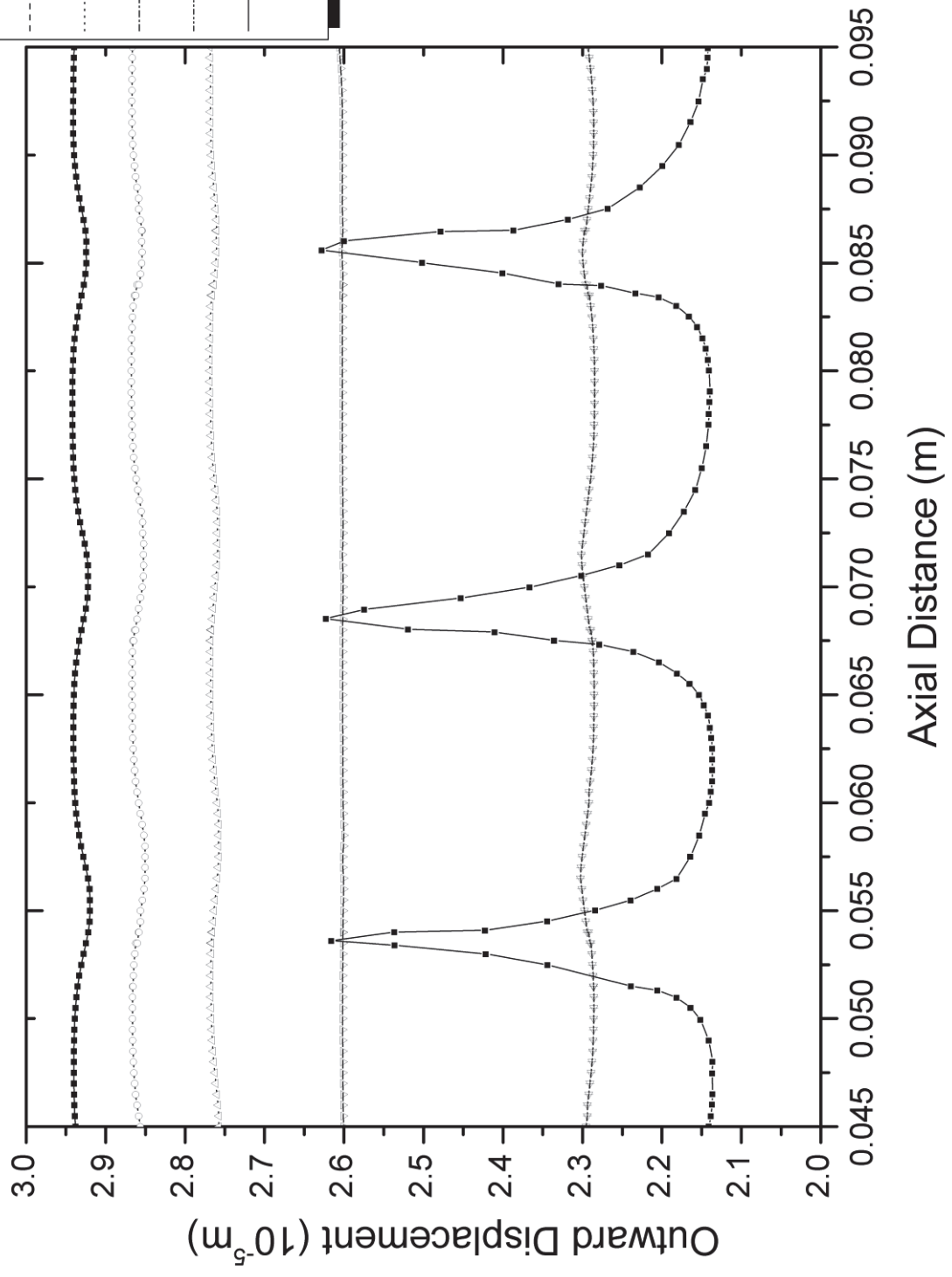
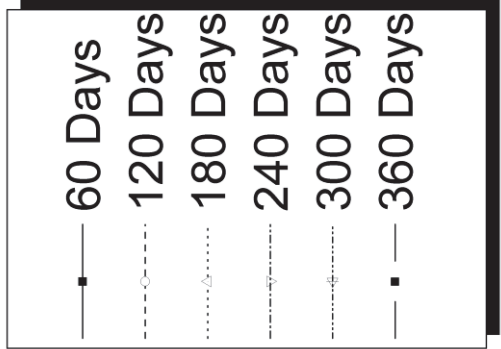


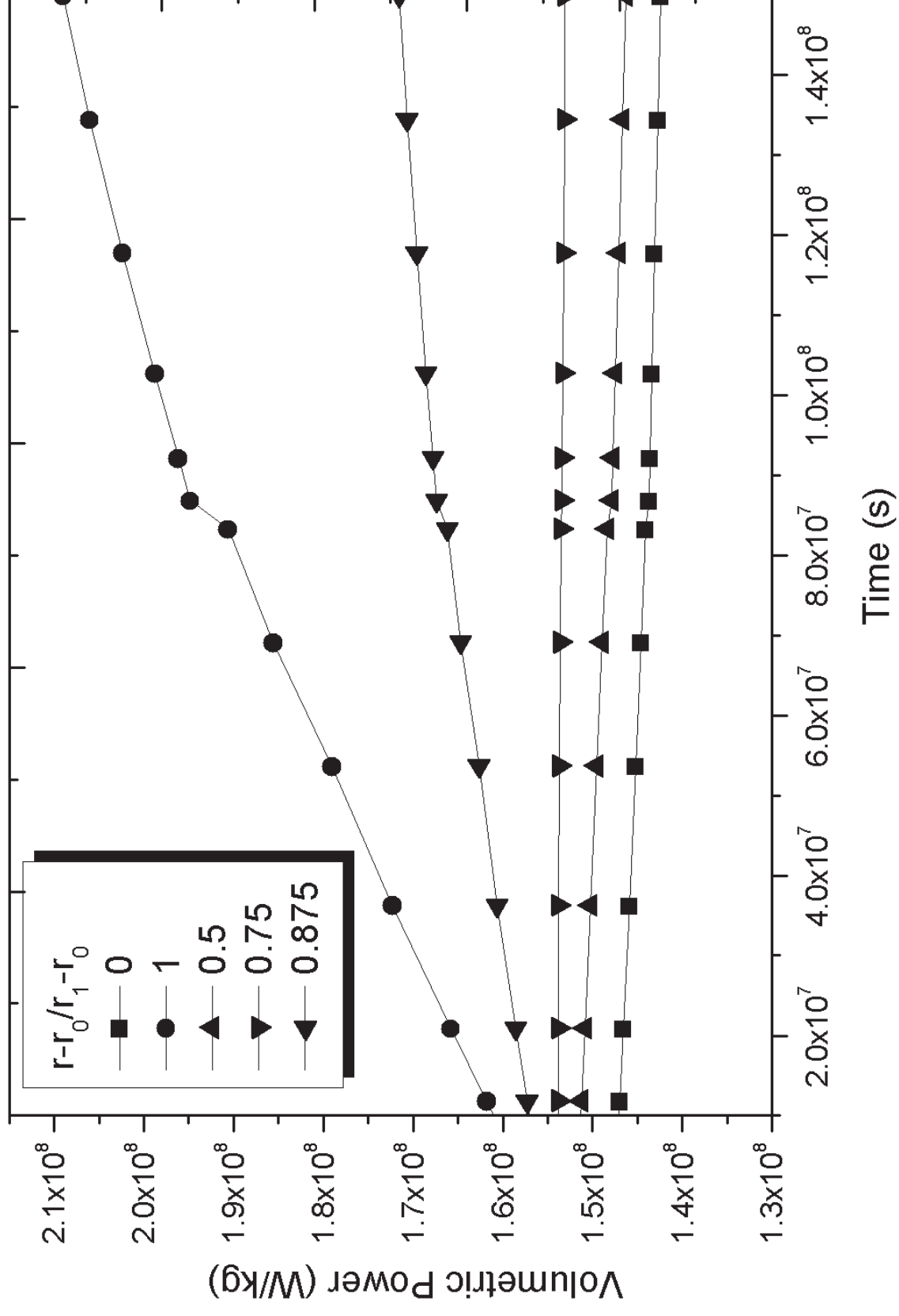


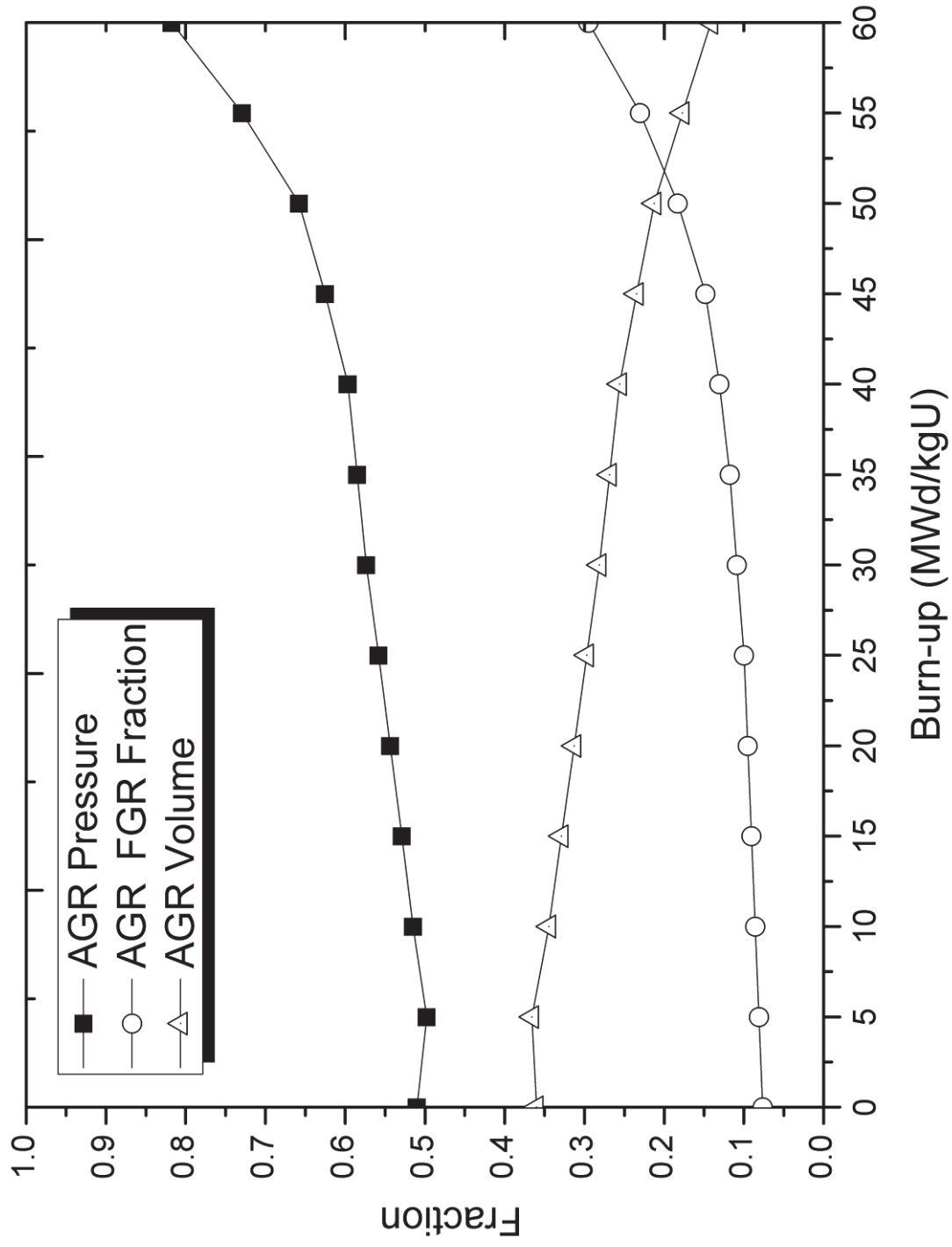


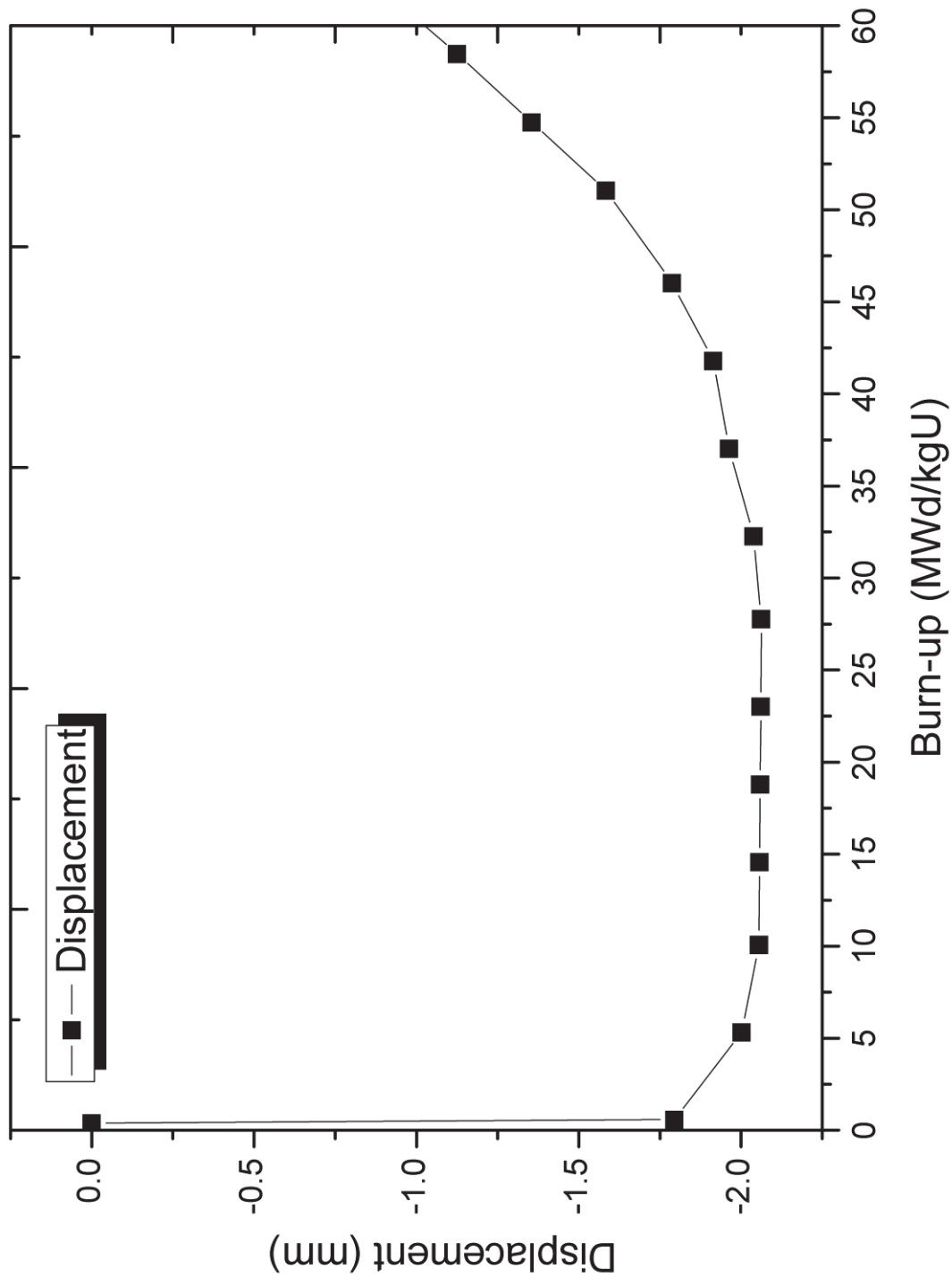


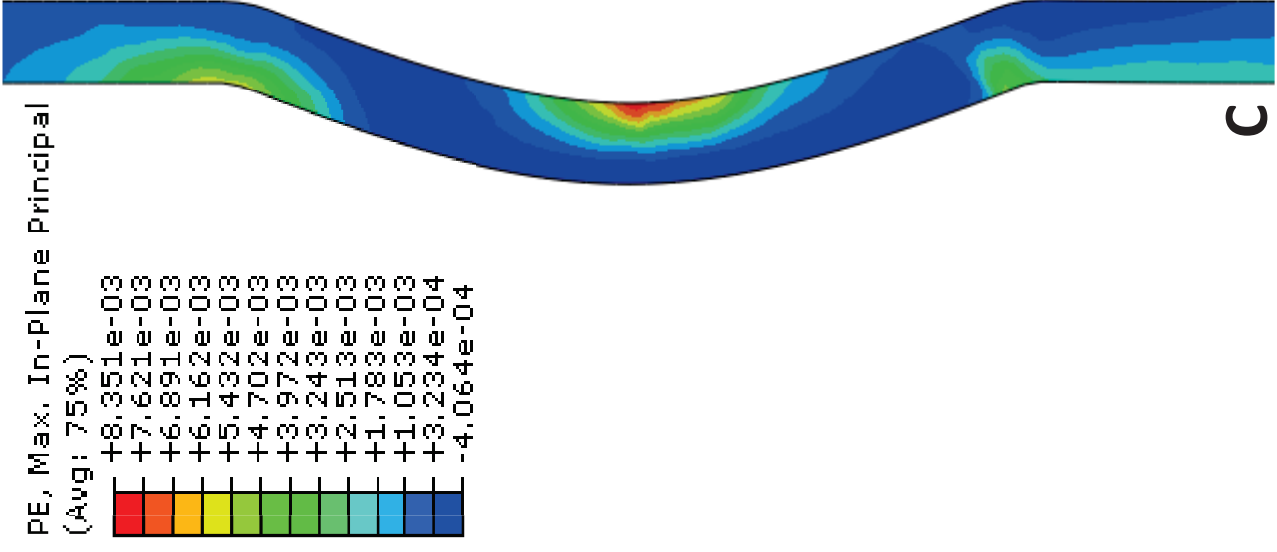
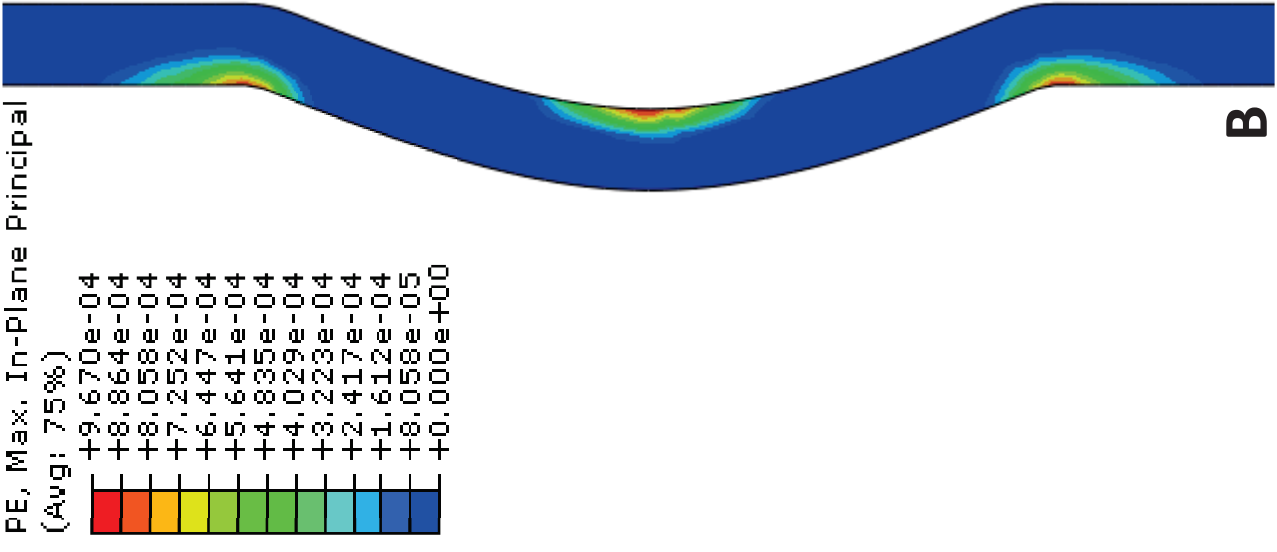
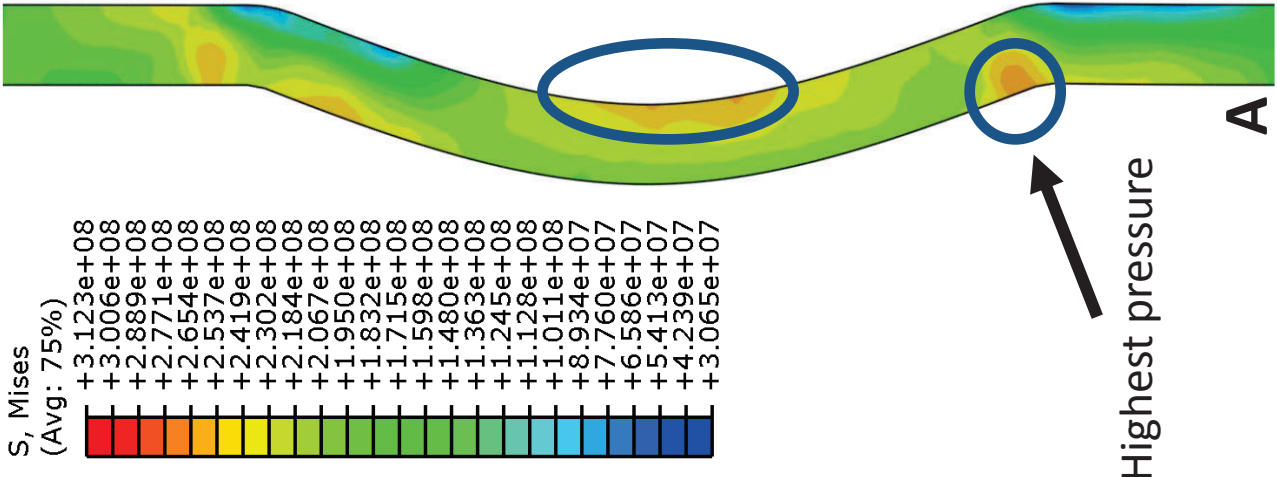


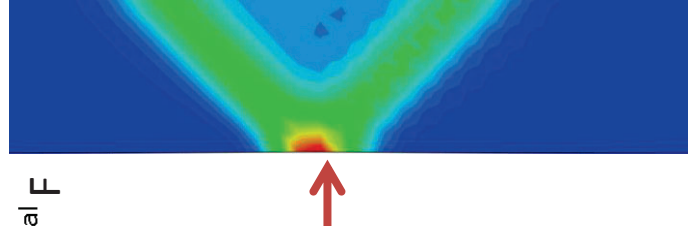
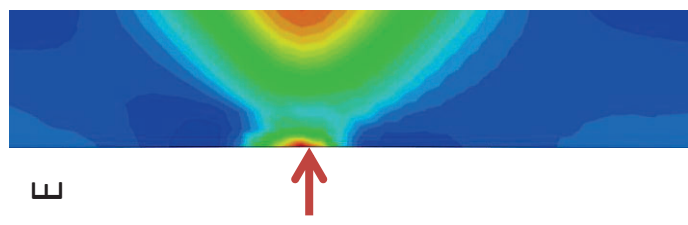
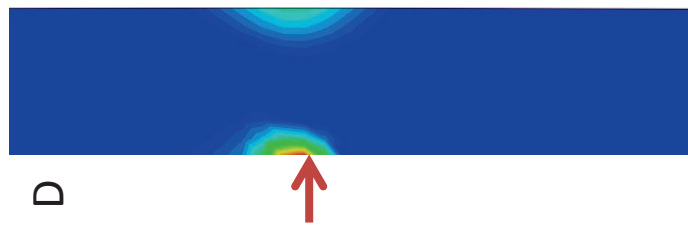
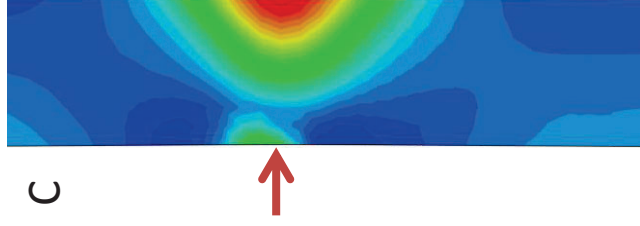
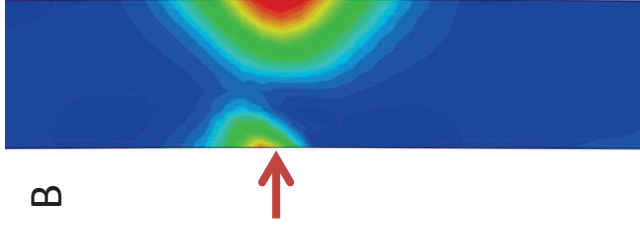
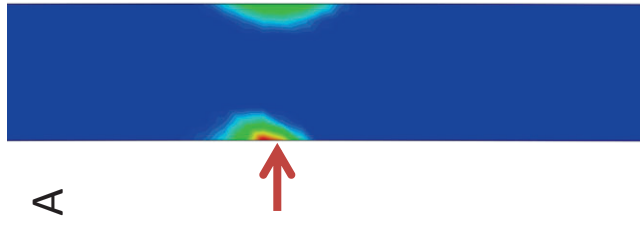


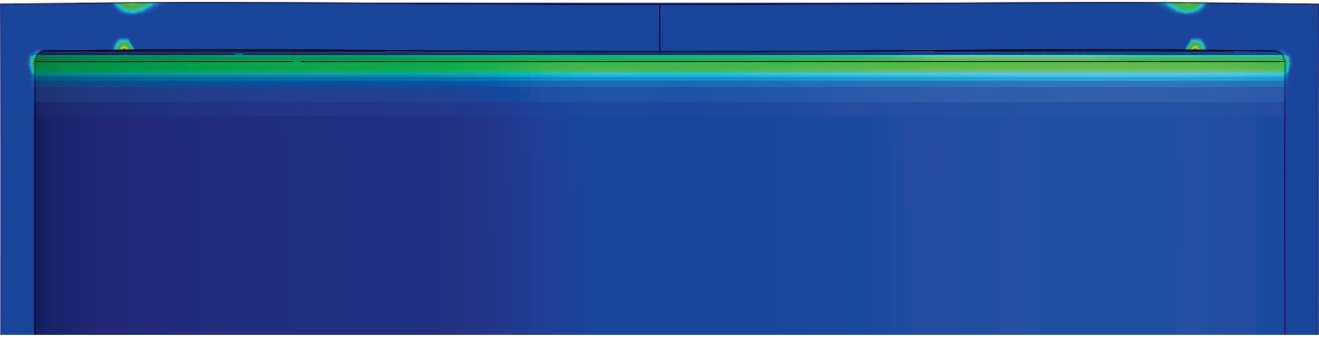
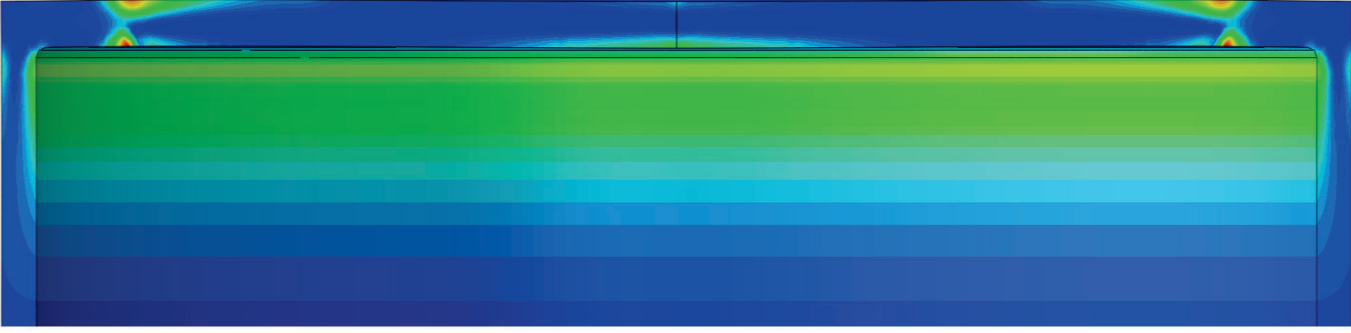
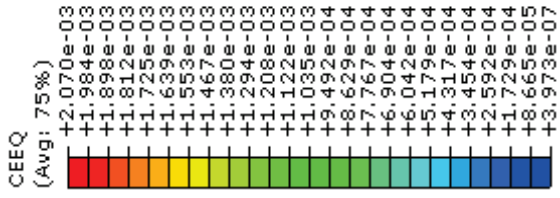
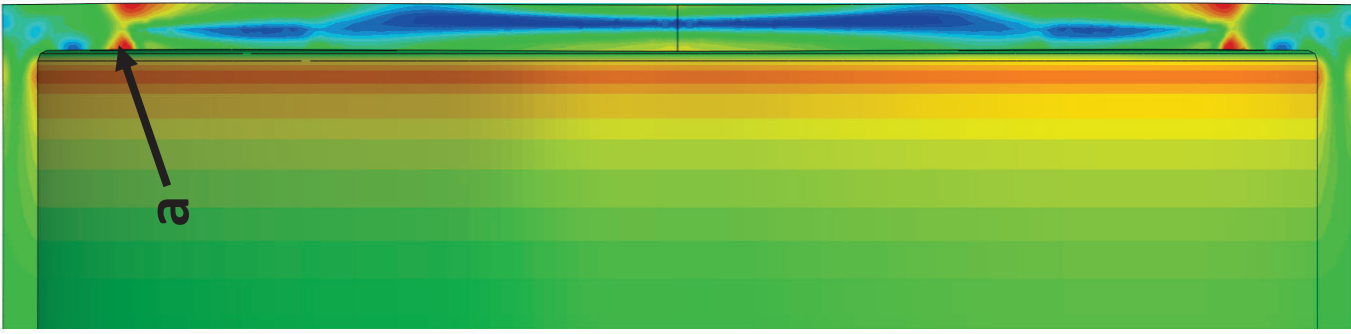
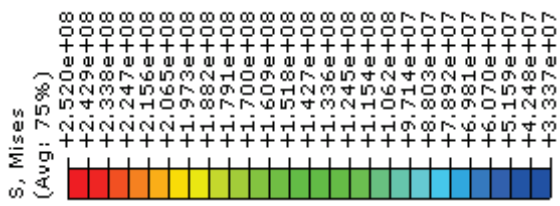












Pin axial direction

A

B

C

